2016 American Control Conference (ACC)
Boston Marriott Copley Place
July 6-8, 2016. Boston, MA, USA

# A Human Foot Motion Localization Algorithm Using IMU

Luan Van Nguyen and Hung Manh La, *IEEE Senior Member*

***Abstract*—Human foot motion localization using inertial measurement unit (IMU) is a challenging problem due to IMU's drift and noise. This paper presents a localization algorithm, which can accurately estimate the position, velocity and attitude of human foot motion based on IMU measurements. The proposed algorithm works efficiently in a real-time and dynamic speed manner. A dynamic Gait Phase Detection (GPD) method is utilized to produce a high accuracy of human foot gait phase detection in dynamic speeds. We then integrate the GDP with an Inertial Navigation System (INS), a Zero Velocity Update (ZVU) and an Extended Kalman Filter (EKF) in a realtime manner to handle the IMU drift problem as well as the noise. Finally, the proposed algorithm is validated and compared with other existing techniques.**

***Index Terms*—Human foot motion localization, EKF, Inertial Navigation System, Gait Phase Detection.**

## I. Introduction

Human foot localization algorithms using Inertial Measurement Unit (IMU) sensors [1]–[4] are promising as the technology is not dependent on installed infrastructure and can be integrated with wearable sensor devices. For instance, IMU has been used for localization and tracking of human motion [5]–[7]. There are different approaches to using IMU for human foot gait phase detection and localization. For example, INS+ ZVU methods are used to deal with IMU drift. Additionally, Extended Kalman Filter (EKF) [2], [4] is applied to increase the accuracy of localization. However, these approaches, especially in environments with local magnetic disturbances, have significant localization errors [2], [3]. Also, current algorithms do not run in real-time and only address certain foot motion speeds. Such limitations can inhibit the practical application of such methods [8]–[10].

This paper presents a development of a dynamic GPD algorithm for accurately detecting human foot gait phases (swing and stance) in dynamic speeds such as walking and running; and a development of a real-time and accurate foot motion localization algorithm. This algorithm integrates the GPD with a ZVU, a Heuristic Heading Reduction (HDR), and an EKF to address IMU's drift and noise.

The remainder of this paper is organized as follows. Section II presents an overview of the human foot motion localization scheme. Section III presents a human gait motion analysis. Section IV presents a real-time human foot motion localization algorithm. Section V presents experimental results to demonstrate the effectiveness of the proposed algorithm, and the comparison with other existing algorithms is given. Finally, the conclusion is given in Section VI.

This work was supported by the University of Nevada, Reno and the National Science Foundation under the grants: NSF-ICorps#1559942 and NSF-NRI#1426828.

L. Nguyen and H. La are with the Department of Computer Science and Engineering, University of Nevada, Reno, NV 89557, USA. Corresponding author: Hung La, email: hla@unr.edu

## II. Overview of Human Foot Motion Localization

The overview of the human foot motion localization scheme with three different modules is shown in Fig. 1.

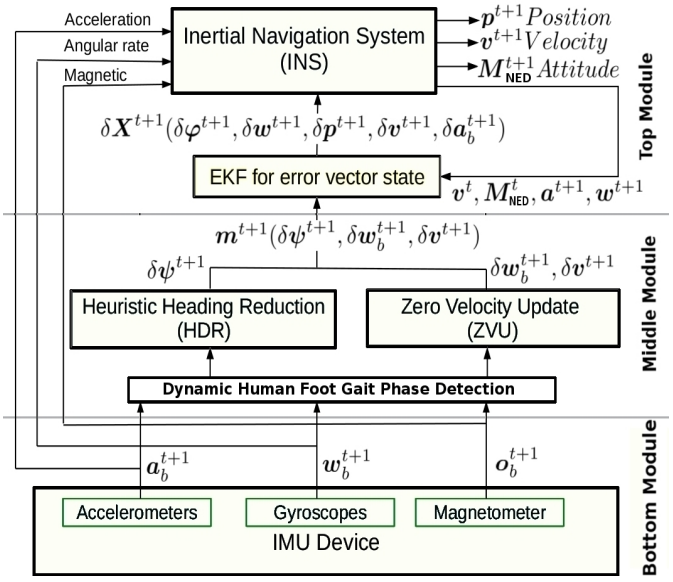


Fig. 1. The INS/EKF ZVU HDR algorithm.

The bottom module is an IMU device including three embedded sensors: Accelerometers measuring the acceleration $\boldsymbol{a}_b^{t+1}$, Gyroscopes measuring the angular rate $\boldsymbol{w}_b^{t+1}$, and Magnetometer measuring the magnetic field of the Earth $\boldsymbol{o}_b^{t+1}$. The subscript $b$ in these formulas refers to the value of these variables in the body frame of the IMU device. The superscript $t+1$ refers to the value of these variables at discrete time $t+1$ in the IMU's time series. Although certain IMU models available on the market integrate the Global Positioning System (GPS), in this paper we are only concerned with the localization algorithm working in environments without the support of GPS.

Since the IMU normally outputs data of the acceleration $\boldsymbol{a}_b^t$, the angular rate $\boldsymbol{w}_b^t$, the Earth magnetic field $\boldsymbol{o}_b^t$, and the quaternion $\boldsymbol{q}^t$, we need to derive the Euler rotation angles, $Roll$ ($\alpha^t$), $Pitch$ ($\beta^t$) and $Yaw$ ($\gamma^t$), from these raw data. Typically, $\alpha^t, \beta^t, \gamma^t$ can be extracted from the IMU's quaternion vector $\boldsymbol{q}^t$ and its conjugation $(\boldsymbol{q}^t)^*$ [11].

The middle module includes three different components: a GPD, a ZVU and a HDR. The GPD detects the stance and swing phases of human foot gait from IMU's data. Then, the ZVU and the HDR utilize the human foot gait detection to estimate the error measurement vector $\boldsymbol{m}^{t+1}$, which is the most important input data for the success of the EKF algorithm. Because the EKF requires kinematically related

measurements of position, velocity and attitude, it has to rely on the important supports from these GPD, ZVU and DHR.

The top module includes an INS and an EKF. The INS system alone can not cope with IMU drift. The EKF with a properly constructed sensor fusion can estimate the IMU biases, therefore it can help the conventional INS reduce the IMU's drift. The EKF estimates the errors of actual acceleration, velocity and position of human foot motion by taking the error measurement vector from the middle module and the feedback data from the output of the INS. In its turn, the INS receives IMU's data and the state measurement errors $\delta \boldsymbol{X}^{t+1}$ from the EKF to continuously compute via dead reckoning the velocity, attitude and position of human foot motion.

## III. Human Gait Motion Detection

This section presents the GPD algorithm to detect human gait phases including stance and swing [12]. Then, a ZVU and HDR are applied to reduce IMU's drift and improve the foot localization.

### A. Dynamic Human Gait Phase Detection (GPD)

First, we present the dynamics of sensor data $d_{g.i}^{t+1}$ at time $t+1$ of the foot step $i_{th}$ from the changes of local acceleration ($|\boldsymbol{a}_{local.i}^{t+1} - \boldsymbol{a}_{local.i}^{t}|$), magnitude of acceleration ($|\boldsymbol{a}_{m.i}^{t+1} - \boldsymbol{a}_{m.i}^{t}|$), and angular rate magnitude ($|\boldsymbol{w}_{m.i}^{t+1} - \boldsymbol{w}_{m.i}^{t}|$):

$$d_{g.i}^{t+1} = |\boldsymbol{a}_{m.i}^{t+1} - \boldsymbol{a}_{m.i}^{t}| + |\boldsymbol{a}_{local.i}^{t+1} - \boldsymbol{a}_{local.i}^{t}| + |\boldsymbol{w}_{m.i}^{t+1} - \boldsymbol{w}_{m.i}^{t}|, \tag{1}$$

where the real motion of acceleration in the North East Down (NED) of the Earth coordinate system [3], [13] can be obtained as:

$$\boldsymbol{a}_{m.i}^{t+1} = \boldsymbol{a}_{e.i}^{t+1} - \boldsymbol{g}_e, \tag{2}$$

where the $\boldsymbol{g}_e$ is the gravitational acceleration vector:

$$\boldsymbol{g}_e = (0.0, 0.0, 9.8m/s^2). \tag{3}$$

and the acceleration of motion in the NED system can be obtained as:

$$\boldsymbol{a}_{e.i}^{t+1} = \boldsymbol{q}^{t+1}.\boldsymbol{a}_{b.i}^{t+1}.(\boldsymbol{q}^{t+1})^*. \tag{4}$$

here $\boldsymbol{a}_{b.i}^{t+1}$ is the acceleration of the IMU in its body frame at time $t+1$ of the foot step $i_{th}$.

The local acceleration $\boldsymbol{a}_{local.i}^{t+1}$ is obtained as:

$$(\boldsymbol{a}_{local.i}^{t+1})^2 = \frac{1}{2f+1} \sum_{j=t-2f}^{t+1} (\boldsymbol{a}_{b.i}^{t+1} - \boldsymbol{a}_{ave.i}^{j})^2. \tag{5}$$

Note that Equ. (5) is computed in real-time. The index $j$ represents data from time step $t+1$ dating back to the previous time steps $2f+1$ (for example, $f$ = 15 steps).

The average acceleration $\boldsymbol{a}_{ave.i}^{j}$ in Equ. (5) is:

$$\boldsymbol{a}_{ave.i}^{j} = \frac{1}{2f+1} \sum_{k=j-2f-1}^{j} \boldsymbol{a}_{b.i}^{k}. \tag{6}$$

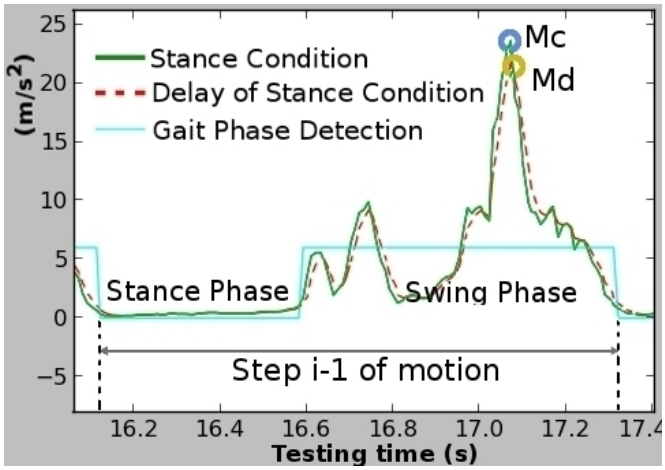


Fig. 2. Human gait phases detection at the foot step i-1.

Then, the dynamic gain $d_{g.i}^{t+1}$ (at time $t+1$ of the foot step $i_{th}$) is used to compute the values of stance condition $s_{c.i}^{t+1}$ from some previous and current values of $d_{g.i}^{t+1}$:

$$s_{c.i}^{t+1} = \frac{d_{g.i}^{t+1} + d_{g.i}^{t} + d_{g.i}^{t-1} + d_{g.i}^{t-2} + d_{g.i}^{t-3}}{5}. \tag{7}$$

Note that Equ. (7) uses five previous and current values of $d_{g.i}^{t+1}$, but this can be changed depending on the type of IMU.

Let's assume that $t+1$ is a discretized time during the foot step $i_{th}$ of the foot motion. The delay of the stance condition $s_{d.i}^{t+1}$ of $s_{c.i}^{t+1}$ is obtained as follows:

$$s_{d.i}^{t+1} = \frac{s_{d.i}^{t-1} + s_{c.i}^{t+1}}{2} \tag{8}$$

where the initial value of $s_{d.i}^{0}$ can be initiated by $0.8$, which is an experimental threshold of normal walking speed.

Let $max_{cd.i}^{t+1}$ be the max changing speed for the difference between $s_{d.i}^{t+1}$ and $s_{c.i}^{t+1}$, and we have:

$$max_{cd.i}^{t+1} = \begin{cases} s_{c.i}^{t+1}, & s_{d.i}^{t+1} \leq s_{c.i}^{t+1} \\ s_{d.i}^{t+1}, & otherwise. \end{cases} \tag{9}$$

Let's define $\boldsymbol{s}_{c.(i-1)}$ as an array of all discretized points $s_{c.(i-1)}^{t+1}$ during the swing phase of the foot step $i-1$ (the green line in the Swing Phase of Fig. 2), and $\boldsymbol{s}_{d.(i-1)}$ as an array of all discretized points $s_{d.(i-1)}^{t+1}$ during the swing phase of the foot step $i-1$ (the red dash line in the Swing Phase of Fig. 2.)

We have a maximum value of the stance condition $s_{c.(i-1)}^{t+1}$ during the swing phase of the foot step $i-1$, $Mc(\boldsymbol{s}_{c.(i-1)})$, computed as:

$$Mc(\boldsymbol{s}_{c.(i-1)}) = Max\{s_{c.(i-1)}^{t+1} | s_{c.(i-1)}^{t+1} \in \boldsymbol{s}_{c.(i-1)}\}. \tag{10}$$

Similarly, the maximum value of delay of the stance condition $s_{d.(i-1)}^{t+1}$ during the swing phase of the foot step $i-1$, $Md(\boldsymbol{s}_{d.(i-1)})$, obtained as:

$$Md(\boldsymbol{s}_{d.(i-1)}) = Max\{s_{d.(i-1)}^{t+1} | s_{d.(i-1)}^{t+1} \in \boldsymbol{s}_{d.(i-1)}\}. \tag{11}$$

The dynamic threshold $th^i$ of the foot step $i_{th}$ is:

$$th^i = Mc(\boldsymbol{s}_{c.(i-1)}) - Md(\boldsymbol{s}_{d.(i-1)}) \tag{12}$$

where the initial value of $th^0$ depends on the IMU sensor, in this case, it is $0.8$, which is an experimental threshold of normal walking speed. In general, for an arbitrary IMU, an initial threshold value can be selected from 0.5 to 1.

From Equ. (12) we can obtain the dynamic human gait detection $g_d^{t+1}$ as follows:

$$g_{d.i}^{t+1} = \begin{cases} 0, & max_{cd.i}^{t+1} \leq th^i \text{ (stance phase)} \\ 6, & otherwise \text{ (swing phase)} \end{cases} \quad (13)$$

when $g_{d.i}^{t+1} = 0$, it is in the stance phase, and when $g_{d.i}^{t+1} = 6$, it is in the swing phase.

### *B. Zero Velocity Update (ZVU) Algorithm*

Once the GPD algorithm has detected a stance phase of human foot motion gait, the ZVU algorithm [1], [2], [4] measures the bias velocity, which helps fix the error of IMU's drifts. Without loss of generality, we can assume that each gait of human foot motion occurs in a duration $[T_i - \delta T_i, T_i]$. Where $T_i$ is a discrete time at the end of the stance phase of the foot step $i_{th}$. The bias error $a_{be}^{t+1}$ of acceleration at time $t+1 = T_i$ of foot motion in the stance phase can be obtained as follows:

$$\boldsymbol{a}_{mbe}^{t+1} = \frac{\boldsymbol{v}_m^{t+1=T_i}}{\delta T_i}. \quad (14)$$

Then, from Equ. (14) the bias error of acceleration in the NED system can be obtained as:

$$\boldsymbol{a}_{ebe}^{t+1} = \boldsymbol{a}_{mbe}^{t+1} + \boldsymbol{g}_e. \quad (15)$$

We now can compute the bias error of acceleration in the IMU body frame as:

$$\boldsymbol{a}_{bbe}^{t+1} = (\boldsymbol{q}^{t+1})^* . \boldsymbol{a}_{ebe}^{t+1} . \boldsymbol{q}^{t+1}. \quad (16)$$

From Equ. (16), we can extract the bias error velocity, which is also the drifted velocity $\delta \boldsymbol{v}^{t+1}$, in the body frame as follows:

$$\delta \boldsymbol{v}_b^{t+1} = \boldsymbol{v}_{bbe}^{t+1} = \int \boldsymbol{a}_{bbe}^{t+1} dt. \quad (17)$$

The actual motion value of acceleration $\boldsymbol{a}_a^{t+1}$, can be calculated by:

$$\boldsymbol{a}_a^{t+1} = \boldsymbol{a}_m^{t+1} - \boldsymbol{a}_{mbe}^{t+1}. \quad (18)$$

The actual velocity and position of the human foot motion can be obtained as follows:

$$\boldsymbol{v}_a^{t+1} = \int \boldsymbol{a}_a^{t+1} dt. \quad (19)$$

$$\boldsymbol{p}_a^{t+1} = \int \boldsymbol{v}_a^{t+1} dt. \quad (20)$$

### *C. Heuristic Heading Reduction (HDR)*

It is notable that the characteristic of human foot motion usually occurs in a straight direction. For this reason, a HDR algorithm [2], [14] is applied to adjust the drifted $Yaw(\gamma)$ angle of heading direction. If the magnetic field of environment makes change in a heading direction, it would effect the bias of $\gamma$ angle. Hence, we can rely on the comparison of the $\gamma$ angle at time step $T_i$ to the two previous $\gamma$ angles at time steps $T_{(i-1)}$ and $T_{(i-2)}$. The result helps to adjust the bias of the $\gamma$ angle as follows:

$$\delta\psi^{t+1} = \delta\psi_{\gamma^{T_i}} = \gamma^{T_i} - \frac{\gamma^{T_{(i-1)}} + \gamma^{T_{(i-2)}}}{2}. \quad (21)$$

where $T_i$ is the last discrete time of the stance phase of the foot step $i_{th}$.

The HDR adjusts the straight bias of the $\gamma$ angle at each discrete time $t+1$ for the acceleration of the swing phase as follows:

$$\delta\psi^{t+1} = \begin{cases} \delta\psi^{t+1}, & \delta\psi^{t+1} \leq th_\gamma \\ 0, & otherwise. \end{cases} \quad (22)$$

where the threshold value ($th_\gamma = 0.5\ rad$) is chosen by the observation of the experiment.

After applying the HDR algorithm, the acceleration at the swing phase of each time step needs to be updated as follows:

$$\boldsymbol{a}_{eHDR}^{t+1} = \boldsymbol{M}_{NED}^{1|0} . \boldsymbol{a}_b^{t+1}. \quad (23)$$

where $\boldsymbol{M}_{NED}^{1|0}$ can be obtained from Equ. (37), but $\alpha$, $\beta$, and $\gamma$ in this equation need to be updated by:

$$\alpha = \alpha^{t+1}, \beta = \beta^{t+1}, \gamma = \gamma^{t+1} + \delta\psi^{t+1}. \quad (24)$$

The real motion acceleration in the NED system is then updated by:

$$\boldsymbol{a}_{mHDR}^{t+1} = \boldsymbol{a}_{eHDR}^{t+1} - \boldsymbol{g}_e. \quad (25)$$

Also, Equ. (19-20) for actual velocity and position need to be computed again by using the new actual acceleration $\boldsymbol{a}_{mHDR}^{t+1}$.

## IV. Real-Time Human Foot Motion Localization Algorithm With Dynamic Speed

In this section, we present a real-time human foot motion localization algorithm applying the proposed GPD method for dynamic gait detection. We named it a Real-Time Dynamic INS/EKF+ZVU+HDR Algorithm. The diagram of this algorithm can be seen in Fig. 3.

In this diagram, whenever the GPD algorithm detects a stance phase at time $t+1$, the ZVU and the HDR algorithms estimate the vector $\boldsymbol{m}^{t+1}$ of the actual error measurement for the EKF's input data as:

$$\boldsymbol{m}^{t+1} = (\delta\psi^{t+1}, \delta\boldsymbol{w}_b^{t+1}, \delta\boldsymbol{v}_b^{t+1}) \quad (26)$$

where the bias of $yaw$ angle $\delta\psi^{t+1}$ is obtained by HDR algorithm as in Equ. (21), the bias error of velocity is obtained as follows:

$$\delta\boldsymbol{v}_b^{t+1} = \boldsymbol{v}_b^{t+1} - \boldsymbol{v}_a^{t+1} \quad (27)$$

where the $\boldsymbol{v}_b^{t+1}$ is obtained by the ZVU algorithm in Equ. (17), $\boldsymbol{v}_a^{t+1}$ is the actual velocity of the foot in the stance phase, or $\boldsymbol{v}_a^{t+1} = [0\ 0\ 0]^T$, and the bias error angular rate is obtained as follows:

$$\delta\boldsymbol{w}_b^{t+1} = \boldsymbol{w}_b^{t+1} - \boldsymbol{w}_a^{t+1} \quad (28)$$

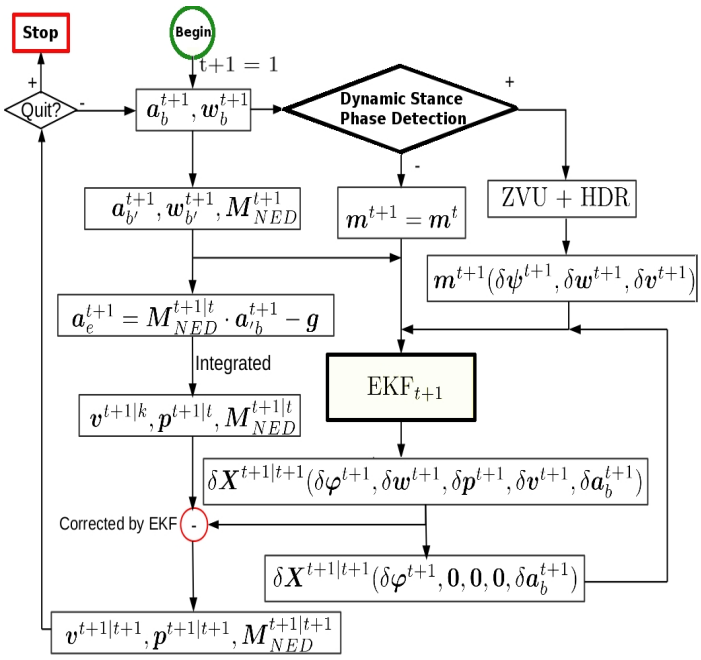


Fig. 3. The Real-Time Dynamic INS/EKF+ZVU+HDR algorithm.

where $\boldsymbol{w}_a^{t+1}$ is the actual angular rate of the foot in the stance phase, or $\boldsymbol{w}_a^{t+1} = [0\ 0\ 0]^T$.

The EKF's error state vector [2], [4] at the previous time $t$ is a 15 element vector $\delta\boldsymbol{X}^{t|t}$, and its function corrects the INS's output values: the velocity, the position, and the attitude as in Fig. 1.

$$\delta\boldsymbol{X}^{t|t} = \delta\boldsymbol{X}^{t}(\delta\boldsymbol{\varphi}^{t}, \delta\boldsymbol{w}^{t}, \delta\boldsymbol{p}^{t}, \delta\boldsymbol{v}^{t}, \delta\boldsymbol{a}_b^{t}) \tag{29}$$

where $\delta\boldsymbol{\varphi}^t$, $\delta\boldsymbol{w}^t$, $\delta\boldsymbol{p}^t$, $\delta\boldsymbol{v}^t$, and $\delta\boldsymbol{a}_b^t$ represent the EKF's estimated errors of the attitude, the angular rate, the position, the velocity, and the acceleration at time $t$.
The EKF's predicted error state vector at time $t+1$ is:

$$\delta\boldsymbol{X}^{t+1|t} = \boldsymbol{\Phi}^{t+1}\delta\boldsymbol{X}^{t|t} + \boldsymbol{n}_p^t \tag{30}$$

where $\delta\boldsymbol{X}^{t|t}$ is the EKF's error state vector at the previous time $t$, and $\boldsymbol{n}_p^t$ is the process noise assumed to be zero mean Gaussian white noise with covariance matrix $\boldsymbol{Q}^t$: $\boldsymbol{n}_p^t \hookrightarrow (0, \boldsymbol{Q}^t)$, $\boldsymbol{Q}^t = \boldsymbol{E}(\boldsymbol{n}_p^t(\boldsymbol{n}_p^t)^T)$.

The EKF's state transition matrix, $\boldsymbol{\Phi}^{t+1}$, is a $15 \times 15$ matrix:

$$\boldsymbol{\Phi}^{t+1} = \begin{bmatrix} \boldsymbol{I} & \Delta t\cdot\boldsymbol{M}_{NED}^{t+1|t} & \boldsymbol{0} & \boldsymbol{0} & \boldsymbol{0} \\ \boldsymbol{0} & \boldsymbol{I} & \boldsymbol{0} & \boldsymbol{0} & \boldsymbol{0} \\ \boldsymbol{0} & \boldsymbol{0} & \boldsymbol{I} & \Delta t\cdot\boldsymbol{I} & \frac{-\Delta t^2}{2}\cdot\boldsymbol{S}(a_{n'}^{t+1}) \\ -\Delta t\cdot\boldsymbol{S}(a_{n'}^{t+1}) & \boldsymbol{0} & \boldsymbol{0} & \boldsymbol{I} & \Delta t\cdot\boldsymbol{M}_{NED}^{t+1|t} \\ \boldsymbol{0} & \boldsymbol{0} & \boldsymbol{0} & \boldsymbol{0} & -\Delta t\cdot\boldsymbol{S}(a_{n'}^{t+1}) \end{bmatrix} \tag{31}$$

where $\boldsymbol{I}$ is a $3 \times 3$ unit matrix, $\boldsymbol{0}$ is a $3 \times 3$ zero matrix. $\boldsymbol{S}(a_{n'}^{t+1})$ is a skew-symmetric matrix of the accelerations:

$$\boldsymbol{S}(\boldsymbol{a}_{n'}^{t+1}) = \begin{bmatrix} 0 & -\boldsymbol{a}_{n'}^{t+1}(2) & \boldsymbol{a}_{n'}^{t+1}(1) \\ \boldsymbol{a}_{n'}^{t+1}(2) & 0 & -\boldsymbol{a}_{n'}^{t+1}(2) \\ -\boldsymbol{a}_{n'}^{t+1}(1) & \boldsymbol{a}_{n'}^{t+1}(0) & 0 \end{bmatrix} \tag{32}$$

where $\boldsymbol{a}_{n'}^{t+1}$ is the bias-corrected acceleration in the NED frame:

$$\boldsymbol{a}_{n'}^{t+1} = \boldsymbol{M}_{NED}^{t+1|t}\cdot\boldsymbol{a}_{b'}^{t+1} \tag{33}$$

here $\boldsymbol{M}_{NED}^{t+1|t}$ is a transformation matrix as in Equ. (35).

The bias compensations for the acceleration $\boldsymbol{a}_{b'}^{t+1}$ and angular rate $\boldsymbol{w}_{b'}^{t+1}$ from the EKF error state vector $\delta\boldsymbol{X}^{t|t}$ in Equ. (29) are obtained as follows:

$$\boldsymbol{w}_{b'}^{t+1} = \boldsymbol{w}_b^{t+1} - \delta\boldsymbol{w}_b^{t+1} \tag{34a}$$
$$\boldsymbol{a}_{b'}^{t+1} = \boldsymbol{a}_b^{t+1} - \delta\boldsymbol{a}_b^{t+1} \tag{34b}$$

where the raw data of the acceleration $\boldsymbol{a}_b^{t+1}$ and the angular rate $\boldsymbol{w}_b^{t+1}$ here is in the IMU's body frame.

The transformation matrix [2], [4], $\boldsymbol{M}_{NED}^{t+1|t}$ that transforms the data from the $IMU$'s body frame into the NED frame is obtained as follows:

$$\boldsymbol{M}_{NED}^{t+1|t} = \boldsymbol{M}_{NED}^{t|t}\cdot\frac{2\boldsymbol{I}_{3\times3} + \delta\boldsymbol{\Omega}_t\cdot\Delta t}{2\boldsymbol{I}_{3\times3} - \delta\boldsymbol{\Omega}_t\cdot\Delta t} \tag{35}$$

where $\delta\boldsymbol{\Omega}_t$ is a skew symmetric matrix of the angular rate:

$$\delta\boldsymbol{\Omega}_t = \begin{bmatrix} \boldsymbol{0} & -\boldsymbol{w}_{b'}^t(2) & \boldsymbol{w}_{b'}^t(1) \\ \boldsymbol{w}_{b'}^t(2) & \boldsymbol{0} & -\boldsymbol{w}_{b'}^t(0) \\ -\boldsymbol{w}_{b'}^t(1) & \boldsymbol{w}_{b'}^t(0) & \boldsymbol{0} \end{bmatrix} \tag{36}$$

where, the $\boldsymbol{w}_{b'}^t$ is computed by Equ. (34a), and the $\boldsymbol{M}_{NED}^{t|t}$ is the last rotation matrix updated by the EKF at the previous step $t$. At the first time, $t+1$ = 1, the $\boldsymbol{M}_{NED}^{1|0}$ is estimated as follows:

$$\boldsymbol{M}_{NED}^{1|0} = \begin{bmatrix} c(\gamma)c(\beta) & c(\gamma)s(\alpha)s(\beta)-c(\alpha)s(\gamma) & s(\alpha)s(\gamma)+c(\alpha)c(\gamma)s(\beta) \\ c(\beta)s(\gamma) & c(\alpha)c(\gamma)+s(\alpha)s(\gamma)s(\beta) & c(\alpha)s(\gamma)s(\beta)-c(\gamma)s(\alpha) \\ -s(\beta) & c(\beta)s(\alpha) & c(\alpha)c(\beta) \end{bmatrix} \tag{37}$$

here $c$, $s$, $\alpha$, $\beta$ and $\gamma$ are $cosine()$, $sine()$, $Roll$ ($\alpha^1$), $Pitch$ ($\beta^1$) and $Yaw$ ($\gamma^1$), respectively.

The EKF's error state at time $t+1$ can be obtained as:

$$\delta\boldsymbol{X}^{t+1|t+1} = \delta\boldsymbol{X}^{t+1|t} + \boldsymbol{K}^{t+1}\cdot[\boldsymbol{m}^{t+1} - \boldsymbol{H}\delta\boldsymbol{X}^{t+1|t}] \tag{38}$$

where $\boldsymbol{K}^{t+1}$ is the Kalman gain defined in Equ. (41); $\boldsymbol{m}^{t+1}$ is defined in Equ. (26) and $\boldsymbol{H}$ is a measurement matrix:

$$\boldsymbol{H}_{7\times15} = \begin{bmatrix} \boldsymbol{O}_{1\times3}^1 & \boldsymbol{O}_{1\times3}^0 & \boldsymbol{O}_{1\times3}^0 & \boldsymbol{O}_{1\times3}^0 & \boldsymbol{O}_{1\times3}^0 \\ \boldsymbol{O}_{3\times3} & \boldsymbol{I}_{3\times3} & \boldsymbol{O}_{3\times3} & \boldsymbol{O}_{3\times3} & \boldsymbol{O}_{3\times3} \\ \boldsymbol{O}_{3\times3} & \boldsymbol{O}_{3\times3} & \boldsymbol{O}_{3\times3} & \boldsymbol{I}_{3\times3} & \boldsymbol{O}_{3\times3} \end{bmatrix} \tag{39}$$

where $\boldsymbol{O}_{1\times3}^1$ = [0 0 1], $\boldsymbol{O}_{1\times3}^0$ = [0 0 0], $\boldsymbol{I}_{3\times3}$ is a $3\times3$ unit matrix, and $\boldsymbol{O}_{3\times3}$ is a $3\times3$ zero matrix.
The EKF's measurement model is defined by:

$$\boldsymbol{z}^{t+1} = \boldsymbol{H}\delta\boldsymbol{X}^{t+1|t+1} + \boldsymbol{n}_z^{t+1} \tag{40}$$

where $\boldsymbol{n}_z^{t+1}$ is the measurement noise with covariance matrix $\boldsymbol{R}^{t+1} = \boldsymbol{E}(\boldsymbol{n}_z^{t+1}(\boldsymbol{n}_z^{t+1})^T)$.

The Kalman gain is obtained as follows:

$$\boldsymbol{K}^{t+1} = \boldsymbol{P}^{t+1|t}\boldsymbol{H}^T(\boldsymbol{H}\boldsymbol{P}^{t+1|t}\boldsymbol{H}^T + \boldsymbol{R}^{t+1})^{-1} \tag{41}$$

where $\boldsymbol{P}^{t+1|t}$ is an estimated error covariance matrix, which is computed at time $t+1$ of the IMU's output sequence:

$$\boldsymbol{P}^{t+1|t} = \Phi^t\boldsymbol{P}^{t|t}(\Phi^t)^T + \boldsymbol{Q}^t \tag{42}$$

where $Q^t$ is a process noise covariance matrix; and the previous $\boldsymbol{P}^{t|t}$ is computed by:

$$\boldsymbol{P}^{t|t} = (\boldsymbol{I}_{15\times15} - \boldsymbol{K}^t\boldsymbol{H})\boldsymbol{P}^{t|t-1}(\boldsymbol{I}_{15\times15} - \boldsymbol{K}^t\boldsymbol{H})^T + \boldsymbol{K}^t\boldsymbol{R}^t(\boldsymbol{K}^t)^T. \tag{43}$$

Now, the acceleration $\boldsymbol{a}_e^{t+1}$ of human motion in the NED frame can be obtained by transforming the bias-compensated acceleration from Equ. (34b) to the NED frame then subtracting the vector $\boldsymbol{g}_e$ from it as follows:

$$\boldsymbol{a}_e^{t+1} = \boldsymbol{M}_{NED}^{t+1|t} \cdot \boldsymbol{a}_{b'}^{t+1} - \boldsymbol{g}_e. \tag{44}$$

The predicted velocity of EKF in the NED frame at time $t+1$ is integrated from an motion acceleration as:

$$\boldsymbol{v}^{t+1|t} = \boldsymbol{v}^{t|t} + \boldsymbol{a}_e^{t+1} \cdot \Delta t. \tag{45}$$

This velocity is integrated one more time to compute the foot position in the NED frame:

$$\boldsymbol{p}^{t+1|t} = \boldsymbol{p}^{t|t} + \boldsymbol{v}^{t+1|t} \cdot \Delta t \tag{46}$$

Finally, we can use the EKF's error state vector in Equ. (38) to adjust the values of the velocity in Equ. (45), the position in Equ. (46), and the attitude in Equ. (35).

$$\boldsymbol{v}^{t+1|t+1} = \boldsymbol{v}^{t+1|t} - \delta\boldsymbol{v}^{t+1|t+1} \tag{47}$$

$$\boldsymbol{p}^{t+1|t+1} = \boldsymbol{p}^{t+1|t} - \delta\boldsymbol{p}^{t+1|t+1} \tag{48}$$

$$\boldsymbol{M}_{NED}^{t+1|t+1} = \frac{2\boldsymbol{I}_{3\times3} + \delta\boldsymbol{\Theta}_t}{2\boldsymbol{I}_{3\times3} - \delta\boldsymbol{\Theta}_t} \cdot \boldsymbol{M}_{NED}^{t+1|t} \tag{49}$$

where:

$$\delta\boldsymbol{\Theta}^t = -\begin{bmatrix} 0 & -\delta\boldsymbol{\varphi}^t(2) & \delta\boldsymbol{\varphi}^t(1) \\ \delta\boldsymbol{\varphi}^t(2) & 0 & -\delta\boldsymbol{\varphi}^t(0) \\ -\delta\boldsymbol{\varphi}^t(1) & \delta\boldsymbol{\varphi}^t(0) & 0 \end{bmatrix} \tag{50}$$

where, $\delta\boldsymbol{\varphi}^t$ is the EKF's error state value for the attitude at the previous time $t$, and it is obtained as in Equ. (38).

## V. Experimental Results

In this section, the proposed algorithm (INS/EKF+ZVU+HDR) is validated by using an external localization system, called Motion Tracking System (MTS) from Motion Analysis Corporation [15]. Then, the proposed algorithm is compared with two other algorithms: the INS/ZVU and the INS/ZVU+HDR. We mount a MicroStrain 3DM-GX3-25 IMU sensor on the shoe for testing them (see Fig. 4 (3)). We implement the algorithms in the C++ language and run them on the Hydro ROS (Robotic Operating System) platform. The real-time stream data from this IMU sensor is processed by the proposed algorithm.

### A. Algorithm Validation with MTS

MTS has a high level of precision, with only sub-millimeter error, and it can be used as the Ground Truth system or an independent and accurate localization system, to validate the proposed algorithm. The difference between the MTS's results and the proposed algorithm's results is the error of the proposed algorithm.

In order to do this validation, we setup the experiment as in Fig. 4. The configuration of this MTS system includes 16 passive optical cameras, which are mounted on the pipe system around the Advanced Robotics and Automation (ARA) lab's walls, as in Fig. 4 (2). Because the shoe needs to be tracked as a rigid body, we attach seven markers on it as in Fig. 4 (3).

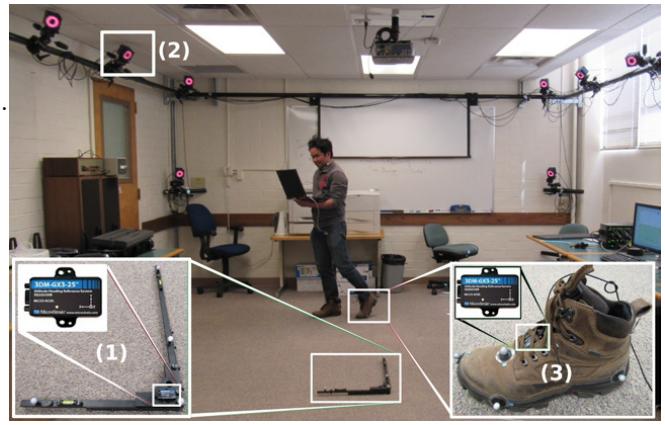


Fig. 4. Using MTS to verify the proposed algorithm.

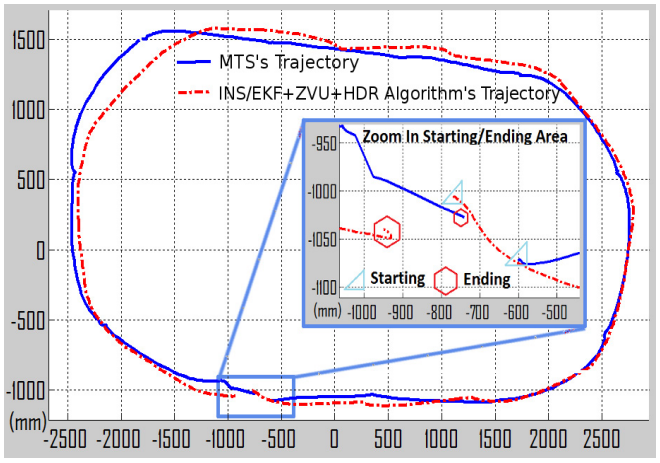


Fig. 5. Plotting trajectories of both MTS and the proposed algorithm.

In Fig. 5, the solid line and dash-dot line are trajectories tracked by the MTS and the proposed IMU algorithm, respectively. The difference between these trajectories is exactly the error of the proposed algorithm. In this validation, the distance difference is 45 mm. The traveling distance in this validation around the ARA lab is 13.4 m. So, the average error in the total traveling distance is approximated a 0.335% error.

### B. Indoor and Outdoor Localization Tests

Fig. 6 shows the comparison results of three algorithms in indoor tests: INS/ZVU, INS/ZVU+HDR and INS/EKF+ZVU+HDR. We can see that the INS/EKF+ZVU+HDR algorithm outperforms the others, since its walking trajectory closely matches the hallway of the SEM building, UNR campus. The average of the different distance between the starting point and ending point in the 2D coordinate for Real-time Dynamic INS/EKF

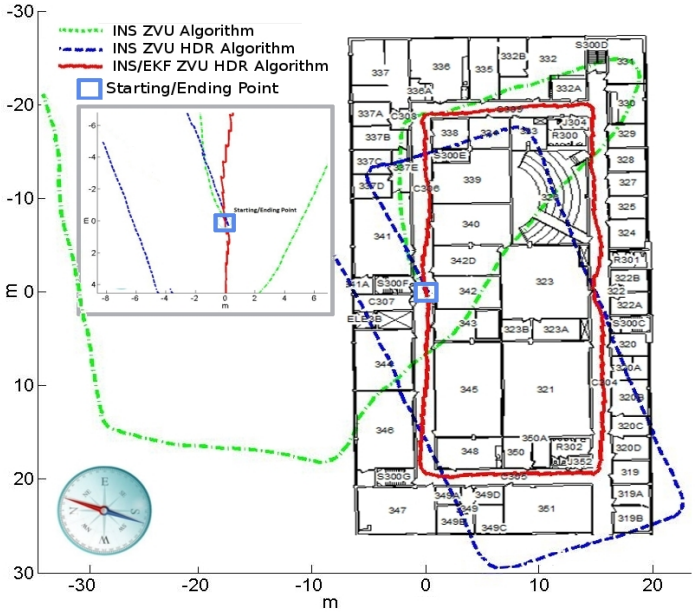


Fig. 6. 2D trajectories plotted on the hallway of the 3rd floor plan in the SEM building, UNR campus.

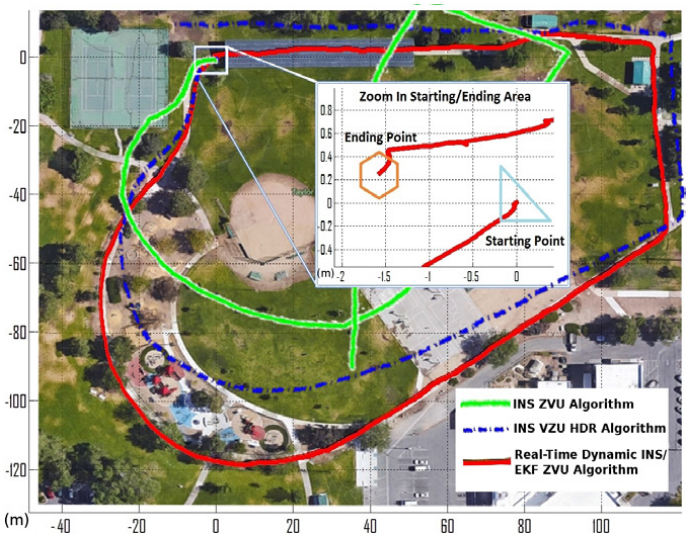


Fig. 7. 2D trajectories of outdoor testing along the sidewalks on the Taylor park in Reno, Nevada.

ZVU HDR algorithm is about $0.45m$ over $120m$, equivalent to $0.375\%$ error.

For outdoor environments, we tested and compared the results of three algorithms: INS/ZVU, INS/ZVU+HDR and INS/EKF+ZVU+HDR in a larger scale trajectory along the sidewalk in the Taylor park in Reno. The results are plotted in Fig. 7. As can be seen, INS/EKF+ZVU+HDR algorithm performed better than the others since the walking trajectory matches the sidewalk very well. The zoom-in area in Fig. 7 shows the starting point and ending point of the walking path on the sidewalk of the Taylor park. The average distance difference between the starting point and ending point in the 2D coordinate for this outdoor testing of the Real-time Dynamic INS/EKF+ZVU+HDR is about $1.7m$ over $512m$, equivalent to $0.33\%$ error.

## VI. Conclusion

This paper has presented a real-time human foot motion localization algorithm, which integrates four different components including the dynamic GPD, the ZVU, the HDR and the EKF. The proposed algorithm has significantly removed the IMU's heading drifts and noise. The algorithm works in real-time and accurately estimate the human foot position, velocity and attitude with dynamic motion speeds. Moreover, it has been validated by an external localization system. To show the effectiveness of the proposed algorithm, localization results have been conducted and demonstrated in both indoor and outdoor environments.

Although the proposed algorithm targets environments without support from other sensors such as GPS, radio tracking systems, cameras, etc., it can be integrated with these sensors to enhance the performance of human foot localization for long traveling distance.

## References


[1] I. Skog, P. Handel, J. Nilsson, and J. Rantakokko. Zero-velocity detectionan algorithm evaluation. *Biomedical Engineering, IEEE Transactions*, 57(11):2657–2666, November 2010.

[2] A.R.Jimenez, F. Seco, J.C. Prieto, and J.Guevara. Indoor pedestrian navigation using an ins/ekf framework for yaw drift reduction and a foot-mounted imu. *IEEE Positioning Navigation and Communication (WPNC), 7th Workshop*, 2010.

[3] X. Yun, J. Calusdian, E. R. Bachmann, and R. B. McGhee. Estimation of human foot motion during normal walking using inertial and magnetic sensor measurements. *Instrumentation and Measurement, IEEE Transactions*, 61(7):2059–2072, July 2012.

[4] E. Foxlin. Pedestrian tracking with shoe-mounted inertial sensors. *IEEE Computer graphics and Applications*, 1:38–46, 2005.

[5] Q. Yuan, I. M. Chen, and S. P. Lee. Slac: 3d localization of human based on kinetic human movement capture. In *Robotics and Automation (ICRA), 2011 IEEE International Conference on*, pages 848–853, May 2011.

[6] F. Hoflinger, R. Zhang, and L. M. Reindl. Indoor-localization system using a micro-inertial measurement unit (imu). In *European Frequency and Time Forum (EFTF)*, pages 443–447, April 2012.

[7] H. Fourati, N. Manamanni, L. Afilal, and Y. Handrich. Position estimation approach by complementary filter-aided imu for indoor environment. In *European Control Conference (ECC)*, pages 4208–4213, July 2013.

[8] L. Nguyen and H. M. La. Development of a smart shoe for building a real-time 3d map. *in Proceedings of The 32st International Symposium on Automation and Robotics in Construction and Mining (ISARC)*, June 2015.

[9] H. M. La, N. Gucunski, S. H. Kee, J. Yi, T. Senlet, and L. Nguyen. Autonomous robotic system for bridge deck data collection and analysis. *Intelligent Robots and Systems (IROS 2014), 2014 IEEE/RSJ International Conference*, pages 1950–1955, September 2014.

[10] L. Nguyen, H. M. La, J. Sanchez, and T. Vu. A smart shoe for building a real-time 3d map. *Automation in Construction (Accepted)*, pages 1–10, Feb. 2016.

[11] L. Nguyen and H. M. La. Real-time human foot motion localization algorithm with dynamic speed. *IEEE Transactions on Human-Machine Systems (Accepted)*, pages 1–12, Jan. 2016.

[12] L. Nguyen, H. M. La, and T. H. Duong. Dynamic human gait phase detection algorithm. *The ISSAT International Conference on Modeling of Complex Systems and Environments (MCSE)*, June 2015.

[13] W. George and II. Collins. *The Foundations of Celestial Mechanics*. The Pachart Foundation dba Pachart Publishing House and reprinted by permission, US, 2004.

[14] J. Borestein, L. Ojeda, and S. Kwanmuang. Heuristic reduction of gyro drift in imu-based personnel tracking system. *SPIE Defense, Security and Sensing Conference*, pages 1–11, April 2009.

[15] Motion tracking system - motion analysis corporation. *http://www.motionanalysis.com*.